The tight junction protein CAR regulates cardiac conduction and cell–cell communication

Ulrike Lisewski,[1] Yu Shi,[1] Uta Wrackmeyer,[1] Robert Fischer,[3] Chen Chen,[1] Alexander Schirdewan,[3,4] Rene Jüttner,[2] Fritz Rathjen,[2] Wolfgang Poller,[4] Michael H. Radke,[1] and Michael Gotthardt,[1,5]

[1]Neuromuscular and Cardiovascular Cell Biology, [2]Developmental Neurobiology, Max Delbrück Center for Molecular Medicine (MDC), 13122 Berlin-Buch, Germany
[3]HELIOS Kliniken GmbH, Franz-Volhard Klinik, Charité, Humboldt University, 13125 Berlin, Germany
[4]Department of Cardiology, Campus Benjamin Franklin, D-12200 Berlin, Germany
[5]Department of Veterinary and Comparative Anatomy, Pharmacology, and Physiology, Washington State University, Pullman, WA 99164

The Coxsackievirus-adenovirus receptor (CAR) is known for its role in virus uptake and as a protein of the tight junction. It is predominantly expressed in the developing brain and heart and reinduced upon cardiac remodeling in heart disease. So far, the physiological functions of CAR in the adult heart are largely unknown. We have generated a heart-specific inducible CAR knockout (KO) and found impaired electrical conduction between atrium and ventricle that increased with progressive loss of CAR. The underlying mechanism relates to the cross talk of tight and gap junctions with altered expression and localization of connexins that affect communication between CAR KO cardiomyocytes. Our results indicate that CAR is not only relevant for virus uptake and cardiac remodeling but also has a previously unknown function in the propagation of excitation from the atrium to the ventricle that could explain the association of arrhythmia and Coxsackievirus infection of the heart.

CORRESPONDENCE
Michael Gotthardt:
gotthardt@mdc-berlin.de

Abbreviations used: AV, atrioventricular; CAR, Coxsackievirus-adenovirus receptor; E, embryonic day; ECG, electrocardiogram; EP, electrophysiology; HV, His-ventricle; MHC, myosin heavy chain.

Altered electrical coupling is a hallmark of cardiac arrhythmia that can result from diverse forms of heart disease (1). Various proteins that form contacts between cardiomyocytes have been linked to arrhythmia both in human patients and in animal models. A specialized cell–cell contact, the gap junction, accounts for the majority of intercellular coupling between cardiomyocytes (2). GAP junctions are formed from connexins (Cx) that assemble into two hemichannels for electric and metabolic cell-to-cell signaling. Mutations of connexins or changes in expression or localization contribute to the development of arrhythmia in patients (3). Connexins form gap junctions with differential gating properties, depending on the isoform composition (4). Thus, the KO of Cx40 leads to atrioventricular (AV) block and bundle branch block (5), whereas, conversely, connexin 30.2 slows AV conduction in mouse heart (4). The activity of gap junctions is not only affected by altered expression or mutations in connexins but also secondary to changes of the adherens junction or the desmosome that can lead to mislocalization and loss of functional gap junctions (6, 7). Unlike gap junction, adherens junction, and desmosome, the tight junction as the fourth type of cell–cell contact at the intercalated disc has so far not been associated with arrhythmia.

The Coxsackievirus-adenovirus receptor (CAR) is a type I transmembrane protein of the tight junction (8). Its extracellular Ig domains mediate homotypic cell adhesion and uptake of adenovirus and coxsackievirus B (9, 10). The cytoplasmic tail is alternatively spliced and interacts with various adaptor proteins that link to signal transduction and endocytosis (8, 11–13). CAR deficiency results in midembryonic lethality

U.L. and Y.S. contributed equally to this paper.
The online version of this article contains supplemental material.

The Rockefeller University Press $30.00
J. Exp. Med. Vol. 205 No. 10 2369-2379
www.jem.org/cgi/doi/10.1084/jem.20080897

with pericardial edema that is related to altered organization of myofibrils and increased proliferation of cardiomyocytes (14–16). This lethality has so far precluded a loss of function analysis in the adult heart. As outlined in the subsequent sections, we have generated a heart-specific inducible CAR KO mouse and found a conduction defect in the AV node as a sign of impaired propagation of excitation from the atrium to the ventricle.

RESULTS

CAR is required for cardiac development

In this paper, we have used a conditional KO approach to investigate the role of CAR in the adult heart. The strategy (Fig. 1) involves the excision of the floxed CAR exon 1 and the tissue-specific expression of the cre recombinase. The myosin heavy chain (MHC) cre transgene is active from midgestation and restricts expression of the cre recombinase to cardiomyocytes (17). We have reduced CAR expression to <20% of control levels at embryonic day (E) 11.5 (Fig. 1 C), which resulted in early lethality between E11.5 and 12.5 (Table I) and resorption from E13.5 (Fig. 1 B). So far, we have not obtained a single KO in >300 offspring from breedings that should produce 25% cardiac KO animals ($MHCcre^{+}$ $CAR^{recf/wt} \times CAR^{recf/recf}$). To circumvent the embryonic lethality, we used expression of the tamoxifen-inducible mutant estrogen receptor fusion protein (MerCreMer; reference 18). After our 2-wk injection regimen (30 mg tamoxifen per kilogram of body weight per day; five injections per week) we achieved a reduction in CAR mRNA levels similar to that of the cardiac KO embryo (Fig. 1 D). CAR mRNA levels declined to <10% from 1 wk after injections. After 2 wk of injections the reduction in protein levels followed (Fig. 1 D).

Loss of CAR leads to impaired electrical conductance from atrium to ventricle

Despite efficient postnatal depletion of CAR, the cardiac-inducible KO animals did not show an obvious phenotype. This includes the initial cardiac assessment by echocardiography that did not show signs of reduced contractile function or dilation in the first month after induction with tamoxifen (unpublished data). The routine monitoring of cardiac activity during anesthesia using the electrocardiogram (ECG) uncovered an unexpected abnormality in the CAR KO hearts (Fig. 2). Although the depolarization and repolarization of the KO ventricle was normal (QRS complex and QT interval), we found that the conduction of the electrical activity from the atrium to ventricle was disturbed. This is reflected in the prolonged PR interval after induction of the KO (Fig. 2, B and C) and corresponds to a problem at the level of the AV node. The PR conduction time increased with progressive deletion of CAR from as early as 1.5 wk after tamoxifen induction (51 ± 4 vs. 39 ± 1 ms; $P < 0.05$; Fig. 2 D) at a time when CAR protein levels started to decline. To exclude an effect of the anesthesia, the analysis was reproduced using telemetry on active animals (Fig. 2 E). The prolongation of the PR interval is the hallmark of first degree AV conduction block (AVB I°),

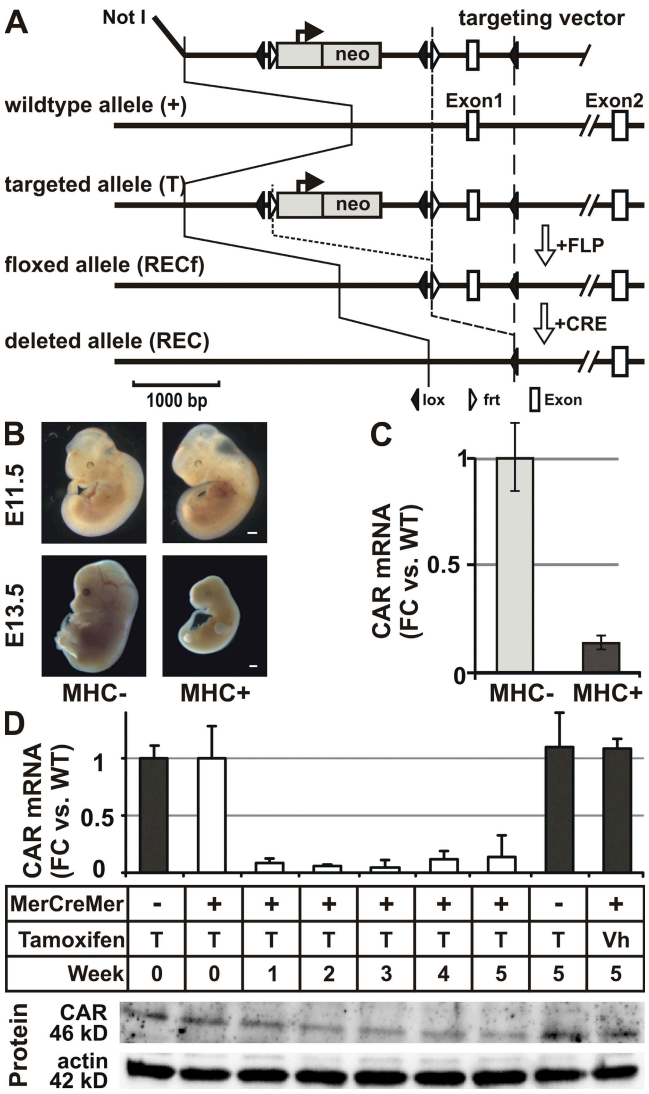

Figure 1. Cardiac-specific CAR KOs. (A) Targeting strategy. Exon 1, which contains the translation start, was replaced with the floxed exon 1 and the FRT-flanked neo cassette. The neo cassette was subsequently removed by germline expression of the FLP recombinase. We generated a heart-specific and an inducible heart-specific CAR KO using the MHC promoter to express the cre recombinase (MHCcre) or the MerCreMer fusion protein (MCMcre), respectively. The latter is activated by the injection of tamoxifen (30 mg per kilogram body weight per day for 2 wk with five injections per week). Bar, 1,000 bp. (B) The heart-specific KO (MHC+) was unaffected through E11.5 with subsequent failure to thrive and death by day 13.5 of gestation (E13.5). Bar, 500 µm. (C) At E11.5, CAR mRNA levels were reduced to 10% of WT levels (FC, fold change). (D) The tamoxifen-inducible heart-specific CAR KO animals can be induced to excise the CAR exon 1. After 1 wk of tamoxifen injections, CAR mRNA expression dropped to <10% in KO animals, and protein levels, as determined by Western blot (CAR compared with actin), followed at 2 wk as compared with two sets of controls, vehicle (Vh)-injected MCM+ or Tamoxifen-treated MCM− animals. Error bars show SD.

which could be documented in all KO animals from week 2 after induction. Blocks of a higher degree were present from 4 wk after induction of the CAR KO (Fig. 2 F), including

Table I. Embryonic lethality of the heart-specific CAR KO

	MHCcre−		MHCcre+	
Age	$CAR^{recf/wt}$	$CAR^{recf/recf}$	$CAR^{recf/wt}$	$CAR^{recf/recf}$
E9.5	1 (20)	1 (20)	1 (20)	2 (40)
E10.5	1 (14)	3 (42)	2 (28)	1 (14)
E11.5	28 (33)	20 (23)	21 (24)	17 (20)
E12.5	16 (47)	8 (24)	9 (26)	1 (3)
E13.5-15.5	12 (48)	5 (20)	8 (32)	0
>Postnatal day 1	95 (30)	137 (43)	85 (27)	0

Shown is the number of tested embryos, with the percentage in parentheses.

partial failure of AV conduction (AVB II°, 25%) or total dissociation of atrial and ventricular rhythms (AVB III°, 37.5%).

Both sinus and AV node are affected in the KO heart

To improve the characterization of the arrhythmia phenotype and to investigate the etiology of the AV conduction defects, we performed in vivo electrophysiological studies in CAR KO (n = 12) and control (n = 11) mice, 4 wk after tamoxifen induction. Examples of different degrees of AV blocks in KO animals are provided in the online supplemental material (Fig. S1, available at http://www.jem.org/cgi/content/full/jem.20080897/DC1). We found no significant difference in atrial and ventricular refractory periods (Fig. 2 F) or inducibility of atrial and ventricular arrhythmias. Adrenergic stimulation did not affect AV conduction in the KO at 4 wk after induction (Fig. S2), but atrial pacing revealed differences in AV conduction capacity in control versus KO animals (Fig. S3). This was determined by the Wenckebach periodicity (AVWB), the longest pacing interval where transient block of AV conduction occurs. In the CAR KO mice, Wenckebach periodicity was observed at slower heart rates.

Between CAR KO and controls, the lengths of P waves and the His-ventricle (HV) intervals (Fig. 2 G) were unchanged. This indicates that CAR regulates AV conduction at the level of the AV node. Additionally, we were able to detect accelerated junctional rhythms (originating from within the AV nodal region) in 50% of CAR KO mice (Table II). The presence of sinus node tachycardia (16.7%) and bradycardia (33.3%) in CAR KO mice indicated an additional effect on sinus node function. Thus, CAR deficiency resulted in binodal disease in 50% of CAR KO mice. To avoid sampling errors and potential effects from anesthesia, we additionally followed the heart rate continuously over time using telemetry (Fig. S4, available at http://www.jem.org/cgi/content/full/jem.20080897/DC1). Heart rate of KO animals maintains a circadian rhythm even with complete AV block and is significantly increased after induction of the KO (from 1 to 2 wk after induction; n = 3 per group).

To find a morphological correlate of the AV block and verify expression of CAR in AV nodal cells, we used various marker proteins to identify the AV node (Fig. 3) and documented differential localization of CAR in cardiomyocytes versus AV nodal cells (Fig. 3, E and F). Although CAR staining was specific to the intercalated disc in ventricular cardiomyocytes, AV nodal cells showed a more diffuse distribution of CAR along the cell membrane.

Despite the early effect on the AV node with total loss of function from week 4, structural changes of the AV node were only minor. Comparisons of sections with identical orientation revealed a small reduction in maximal AV node area in KO animals (Fig. 4 A). Three dimensional reconstruction was used to quantify the corresponding volumes with a <30% reduction of AV node volume in KO ($6.2 \pm 1.9 \times 10^6$ μm^3) versus control mice ($10.9 \pm 1.6 \times 10^6$ μm^3) at 8 wk after induction (Fig. 4, B vs. C). Results were reproduced in two independent experiments (n = 4).

Cross talk of tight and gap junction

In the absence of a major anatomical or structural defect, we used a functional approach to explore the mechanism underlying the conduction block. To analyze the activity of gap junctions, which have previously been implied in isolated AV conduction disease (5, 19), we have adapted a dye-coupling assay to be used on cardiac slices using carboxyfluorescein, which facilitated the detection of coupling in myometrial cells as compared with lucifer yellow (20). This assay enabled us to investigate cell–cell communication between cardiomyocytes in situ. In parallel with the reduction of CAR protein levels, cellular exchange of the fluorescein dye increased from weeks 2–4 (Fig. 5, A and B). The area covered by dye-filled cells after 4 min was used to quantify coupling efficiency. Although coupling was not significantly different between WT and CAR KO cardiomyocytes at week two after initiating tamoxifen injection, dye spread increased significantly from week 3 (Fig. 5 B).

Because the dye-coupling experiments indicated a problem in cell–cell communication, we followed the structure and protein composition of the intercalated discs and the expression and localization of gap junction proteins. CAR KO cardiomyocytes maintained intercalated discs with a normal ultrastructure that did not show widened gaps between cells or increased folding (Fig. S5, available at http://www.jem.org/cgi/content/full/jem.20080897/DC1).

To determine which genes contribute to the development of the AV block phenotype, we have obtained preliminary expression profiling data from mouse atria that show the expected down-regulation of CAR (>10-fold down in the KO)

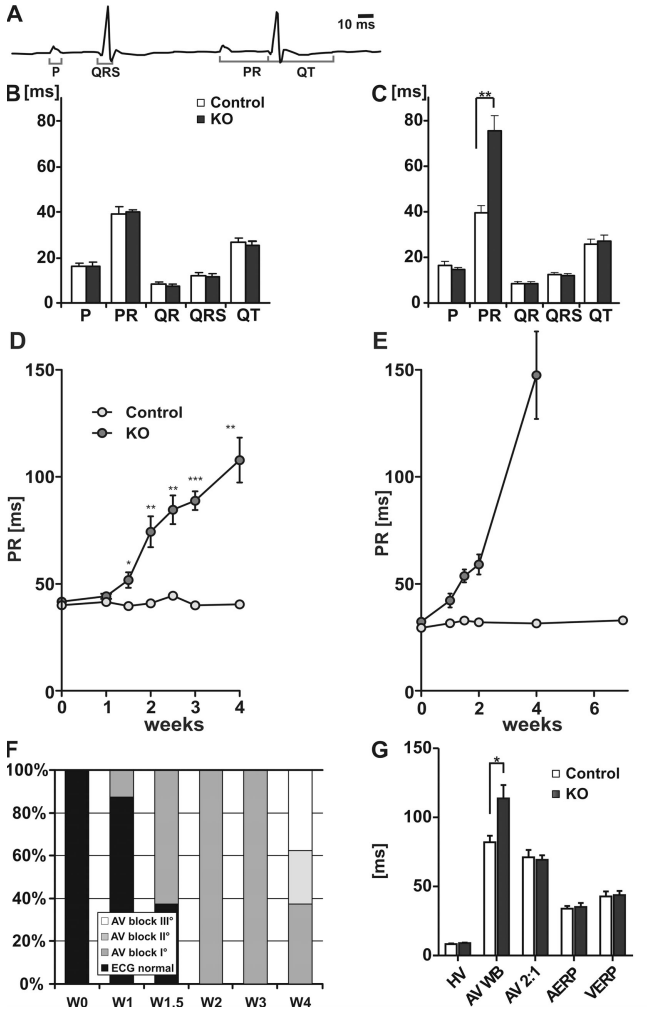

Figure 2. Electrical conduction from atrium to ventricle is impaired in CAR KO hearts. (A) Annotated ECG curve. The PR interval corresponds to the time between atrial and ventricular depolarization. (B and C) Quantification of the ECG changes in KO and control animals before (B) and after (C) the 2-wk treatment with tamoxifen (n = 8 per group; D) revealed an increased PR interval in induced KO animals (n = 8 per group). (E) This finding was reproduced by telemetry to exclude an effect of the anesthesia (n = 3 per group). After week 6, all KO animals showed a complete block so that a PR interval could not be derived. (F) The increased PR interval is the ECG correlate of an AV conduction block. Grading the conduction defect in normal AV conduction versus AV block I to III shows the increase in conduction defects over time with third degree AV blocks at week 4 after induction of the KO. (G) As determined by EPS catheter at week 4 after induction, the HV interval, AV node 2:1 conduction capacity (AV 2:1), atrial effective refractory period (AERP), and ventricular effective refractory period (VERP) were unchanged between genotypes, which would exclude an affliction downstream of the HIS bundle. The only significant change was detected in the interval at which electrical propagation from atrium to ventricle was skipped for the first time (Wenckebach Periodicity [AV-WB]) with a significant increase in the KO heart. *, $P \leq 0.05$; **, $P \leq 0.01$; ***, $P \leq 0.001$. Error bars show SEM. W, week.

and suggest a specific role of connexin 43. The expression of other proteins previously implied in arrhythmia (channels, connexins, and transcription factors) was largely unchanged (unpublished data). We extended the expression analysis to cardiac ventricle (where differences in coupling were documented) and found that RNA levels of both cell–cell contact and adaptor proteins were altered secondary to loss of CAR (Fig. 6). This includes reduced expression of ZO-1, an adaptor protein that binds both CAR and connexins (Fig. 6 A) (8, 21). Expression of connexins was differentially affected in the CAR KO heart. On the mRNA level, Cx45 expression was reduced only late in the development of the phenotype, whereas Cx37 and 40 changed only transiently (Fig. 6, B and C). The altered protein levels of Cx45 and Cx43 (both >40% reduction) in KO hearts compared with Cx40, which was unchanged (Fig. 6 D), indicate a selective effect of CAR on a subset of connexins.

Protein composition of the intercalated disc was analyzed in isolated cardiomyocytes at 8 wk after induction of the phenotype. Costaining with α-actinin antibodies confirmed the proper orientation of the myofilament and connection to the intercalated disc (Fig. 7 A). Although the structure of the intercalated discs was maintained, protein composition changed in response to the loss of CAR. Although the expression and localization of the adherens junction protein N-cadherin was unaffected (Fig. 7 B), the localization of the gap junction protein Connexin 43 (Cx43) was altered in KO cardiomyocytes 8 wk after induction (Fig. 7 C). Reduced amounts of protein were accumulated in subdomains within the intercalated disc of the KO. This observation indicates a functional link between the tight and gap junctions, but not between tight and adherens junctions, that involves CAR.

DISCUSSION

To better understand the function of CAR in the adult heart, we generated an inducible KO. Excision of exon 1, which contains the transcription and translation start, affects the expression of any CAR isoform, whereas the tight control of recombination by tamoxifen eliminates developmental effects that might arise from the embryonic loss of CAR expression. The embryonic lethality has been established for both the KO of CAR exon 1 and exon 2 (14, 15). An additional independent heart-specific KO of CAR exon 2 resulted in a mild hypertrophy phenotype and enabled survival of ∼20% of cardiac KOs (16).

All CAR splice variants described so far, including the soluble isoforms, contain both exons 1 and 2 (22, 23). Thus, both loss of the start codon and transcription start in the KO of exon 1 (15) (our approach) versus the frameshift resulting from the deletion of exon 2 (14, 16) should cause similar phenotypes. Unexpectedly, our heart-specific KO of CAR exon 1 was 100% lethal using the identical α-MHCcre transgene that resulted in 20% survival of the KO of exon 2 (Table I). Both differences in the genetic background and alternative splicing that result in a partial rescue of the exon 2 KO could explain those discrepancies. As compared with our animal model, the heart-specific KO of exon 2 had mild cardiac atrophy of incomplete

Table II. Characterization of conduction defects by EP catheter

	Control	KO
Normal	11 (100)	0
AV conduction defects	0	12 (100)
AVB I°	0	3 (25)
AVB II°	0	1 (8)
AV dissociation/AVB III°	0	8 (67)
Sick sinus syndrome	0	6 (50)
Sinustachycardia	0	2 (17)
Sinusbradycardia	0	4 (33)
Accelerated JR	0	6 (50)

AVB, AV block; Accelerated JR, accelerated junctional rhythms. Percentage is shown in parentheses.

penetrance (ventricular thickening and underdeveloped valves). In our animals, there was no ventricular thickening or malformations of the valves but pericardial effusion. Animals developed a beating heart but died with 100% penetrance. To efficiently produce surviving heart-specific CAR KO animals and generate an adult KO model without a potentially complicating developmental phenotype, we restricted our analysis to the inducible heart-specific KO.

The intercalated disc contains four different types of intercellular junctions, three of which have been linked to cardiac arrhythmia in human and animal models: gap junctions (with connexins forming channels for ion transfer), adherens junctions (with N-cadherin stabilizing gap junctions), and desmosomes (structural organization of the intercalated disc). Proteins of the adherens junction and the desmosome affect conduction, in part indirectly through gap junctions, whose role in the cardiac conduction system is well established. Our results indicate that the proper interplay of all known cell–cell contacts, including the tight junction, determines the electrical properties of the adult heart. Loss of the tight junction protein CAR leads to severe AV block but leaves the electrical properties of the atrial and ventricular myocardium remarkably unaffected. Detailed characterization of the electrical activity of KO hearts revealed no difference in atrial depolarization, so that we can exclude slowed atrial conduction as a reason for the delayed AV conduction (increased PR interval). Physiologically, the PR interval is mainly determined by the conduction through the AV node followed by the His-Purkinje bundles. As the HV interval was equal in CAR KO and control mice, we conclude that CAR regulates AV conduction directly within the AV node. Although AV conduction is impaired, CAR KO mice showed a significantly increased mean heart rate compared with controls at week 4 after induction (Fig. S2), which was confirmed by telemetry of nonanesthetized animals (Fig. S4). In the early stages of AV conduction disease with prolonged, but stable, 1:1 AV conduction, the elevated heart rate results from increased sinus rates that determine the beating frequency. At later stages, accelerated junctional rhythms (originating from within the AV nodal region) cause the tachycardia in KO animals.

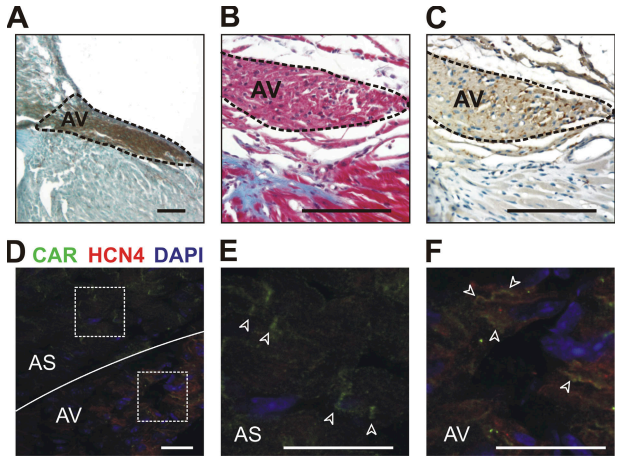

Figure 3. CAR expression in the AV node. (A) The AV node was localized by staining for AChE enzyme activity. (B) Trichrome staining revealed the fibrous body (blue), an anatomical landmark which facilitates localization of the juxtaposed AV node. (C) The identification was confirmed in serial sections by anti-ChAT immunohistochemistry. Bars, 100 µm. (D) Expression of CAR in the AV node was detected by staining with anti-CAR (green) and anti-HCN4 (red) antibodies. The squares indicate the region that is magnified in E and F. (E) CAR is localized in the intercalated disc (arrowheads) within the atrial septum (AS). (F) In cells of the AV node, CAR is distributed along the membrane (arrowheads). Bars, 25 µm.

To exclude a basic structural problem as the basis of the electrical phenotype, we used histology and 3D reconstruction and compared AV nodes from CAR-KO and control hearts. By itself, the minor reduction in size in the absence of fibrosis or fatty infiltration as compared with patients with AV disease could not explain the severity of the arrhythmia (24).

Toward understanding the molecular mechanism underlying the AV block phenotype, we compared our KO to published animal models with arrhythmia that involves prolonged PR intervals (Table III). With the severe AV block in the absence of atrial or ventricular arrhythmia mimicked in the Cx45 KO, we hypothesized that CAR (as described for N-cadherin; reference 6) affects electrical conduction indirectly through gap junctions. Because the size of the murine AV node prevents functional studies of the AV nodal cells, we investigated gap junction activity in cardiomyocytes as a

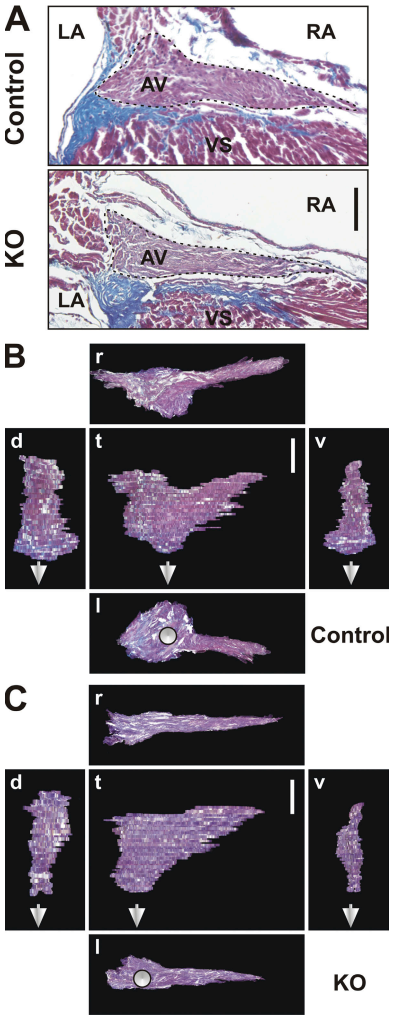

Figure 4. Reduced size of the AV node in the adult CAR KO heart. (A) Masson's Trichrome staining of a KO and control heart at 8 wk after induction shows connective tissue of the valves in blue to separate the AV node area and ventricular septum (VS). To facilitate orientation, left and right atria (LA and RA, respectively) are indicated. The largest AV node area of a series of serial section is slightly reduced in the KO heart compared with the control. (B and C) Three dimensional reconstruction of the AV node from control (B) and CAR KO (C) animals was used to obtain projections in different plains (t, top; l, left; r, right; d, dorsal; v, ventral). The reduced thickness of the AV node results in a volume that corresponds to ~2/3 of the volume of the control AV node ($n = 4$). The continuation of the HIS bundle is indicated by white arrows. Bars, 100 µm.

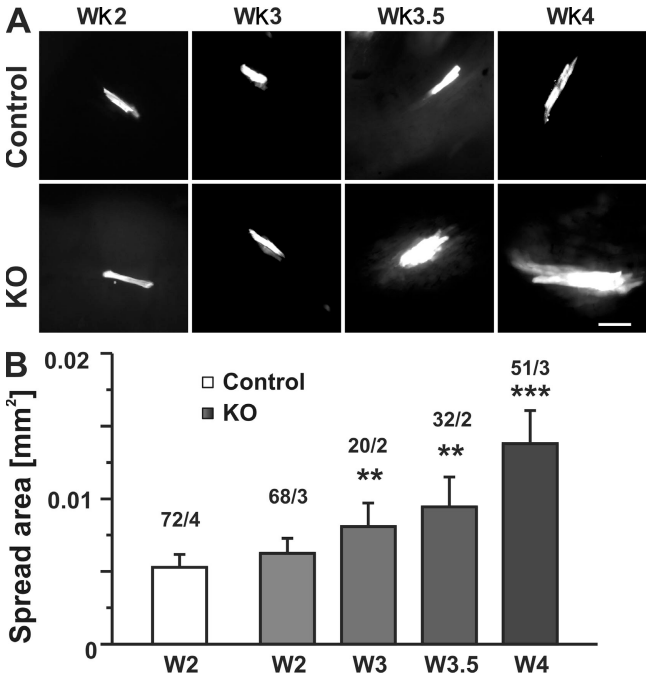

Figure 5. Altered cell–cell communication in the CAR KO heart. (A) After injection of fluorescein, the dye is passed to neighboring cells. Representative cells from KO and control cardiac slices from weeks 2–4 after induction of the KO are shown. The increased longitudinal and lateral coupling is most prominent in cardiac slices at the 4-wk time point. (B) Quantification of >200 injections representing 14 independent hearts documents the significantly increased coupling from week 3 after induction of the KO. The area at the end of the 4-min injection period was used to compare cell–cell communication at the indicated times. For each time point, the number of injections and number of animals is provided (injections/animals). **, $P \leq 0.01$; ***, $P \leq 0.001$, Mann-Whitney test. Error bars show SEM. Bar, 100 µm.

proof of concept. Although dye coupling is widely used to study gap junctions in cultivated cardiomyocytes (7), we have adapted the method to be used in cardiac slices, which largely preserves the structures required for intercellular communication. We found increased dye coupling from week 3 after induction of the KO, indicating cross talk of the tight and gap junction (Fig. 5). Thus, CAR might affect conduction through altered compartmentalization of connexins. A similar dependence has been shown for N-cadherin and connexins with decreased expression of Cx40 and 43 in the N-cadherin KO heart (6). On a molecular level, the functional interaction of gap and tight junction is supported by coprecipitation and colocalization of Cx40 and Cx43 with tight junction molecules occludin, claudin-5, and ZO-1 in endothelial cells (25).

The increased dye coupling does not lead to altered electrical properties of the atrium or ventricle in the CAR KO. This indicates that CAR KO cardiomyocytes, unlike AV nodal cells are not limited by GAP junction activity, a feature which could derive both from altered expression of connexins and differential localization of CAR between the cell types (Fig. 3). AV conduction is altered in various connexin KO animals, such as the cardiac KO of Cx45 (26) or the KO of Cx40, which displays a combination of intraatrial block, ectopic rhythms, and altered atrial propagation in the right atrium (27). None of the ectopic rhythms described in the Cx40 KO or of the spontaneous or the inducible ventricular tachyarrhythmias of the Cx43 KO (28) could be detected in the CAR KO heart. These results indicate a residual function of Cx40 and Cx43 in the CAR KO and further underscore the specific role of CAR in AV conduction. In part, this is reflected in the differential expression of connexins in the KO heart: Cx40

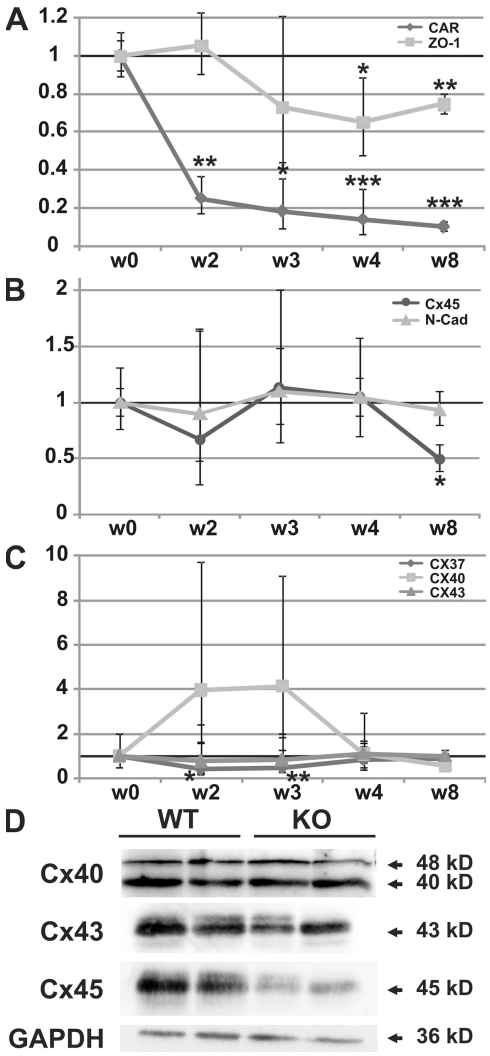

Figure 6. Altered expression of the cell–cell contact proteins in CAR KO hearts. (A) Expression of the CAR and its adaptor protein ZO-1 were reduced significantly from weeks 2 and 4, respectively, after induction of the KO. (B) The composition of the GAP junction was altered as a result of differential expression of Cx37 (transiently reduced) and Cx40 (transiently increased, albeit not significantly). Expression of Cx43 was unchanged. (C) Cx45 was the only connexin with RNA levels significantly altered late in the progression of the phenotype (reduced from >8 wk). The adherens junction protein N-cadherin was unchanged. All expression data were normalized to GAPDH and levels at week 0 (before induction) were set to 100%. Fold change is shown on the y-axis. $n = 3$ per group. Error bars show SD. (D) Cardiac expression of Cx40, Cx43, and Cx45 was confirmed on the protein level with down-regulation of Cx43 and Cx45, but not Cx40, in animals at >8 wk after induction of the phenotype. GAPDH was used as a loading control. After normalization to GAPDH, Cx45 levels were reduced by 45% ($P = 0.012$), Cx 43 levels by 43% ($P = 0.015$), and Cx40 levels were not changed significantly ($n = 4$). *, $P \leq 0.05$; **, $P \leq 0.01$; ***, $P \leq 0.001$.

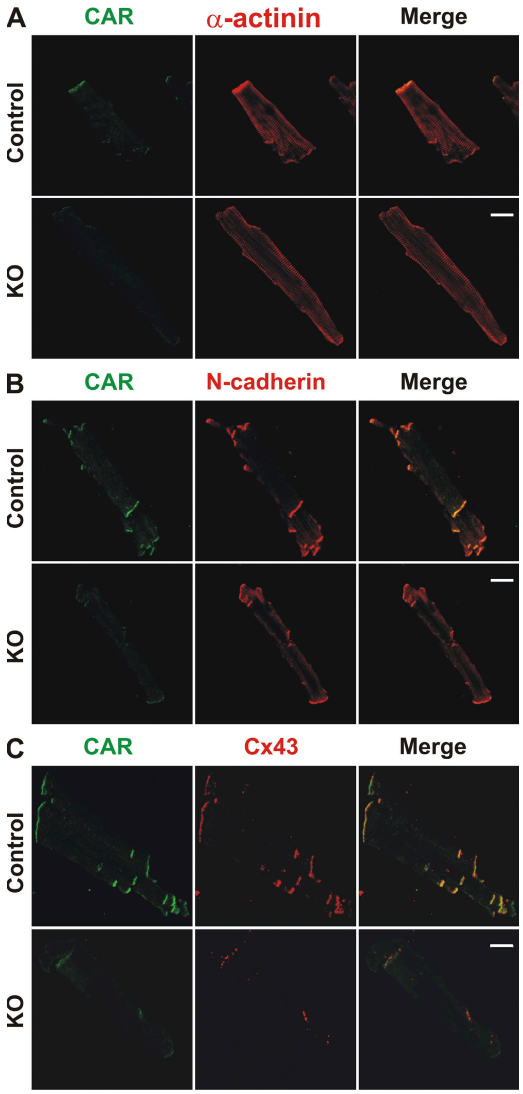

Figure 7. Localization of connexin 43 is dependent on CAR. In the absence of CAR, intercalated discs are maintained with proper localization of N-cadherin but changes in expression and localization of Cx43. (A) Staining with anti-CAR and anti–α-actinin antibodies shows the proper localization of CAR in WT cardiomyocytes and correct orientation of the myofilaments. In KO cells, specific CAR staining was reduced to <10% compared with WT cardiomyocytes. (B) Staining with anti-CAR and anti–N-cadherin antibodies documents the proper expression and localization of N-cadherin upon deletion of CAR. (C) Staining with anti-CAR and anti-Cx43 antibodies reveals that Cx43 expression is reduced in KO cardiomyocytes 8 wk after induction. Residual Cx43 protein is localized in subdomains within the intercalated disc. Comparable results were obtained in three independent experiments. Bars, 20 µm.

protein levels are maintained at physiological levels, whereas Cx45 expression is reduced in the KO heart. Together with the functional analysis indicating that Cx40 or Cx45 are affected in the CAR KO (both share the AV block phenotype with the CAR KO), the expression analysis suggests that the effect of CAR is mediated by Cx45.

In the mouse model, it is challenging to study the AV node and even more difficult to study the sinus node (with hardly any literature data available). Thus, we focused our molecular and morphological analysis on the AV node and cardiac ventricle. The documented cross talk of CAR and

Table III. Conduction phenotypes with prolonged PR interval

Gene	Protein	Model	Conduction defects in addition to AV block
Cacna1d	L-type Ca channel	KO	Abnormal QRS; sinus arrhythmia (41)
Egf-R	EGF-Receptor	KO	Abnormal QRS; prolonged QT (42)
EphA3	Eph receptor A3	KO	Bradycardia (43)
Cx40	Connexin 40	KO	Prolonged P, QT; abnormal QRS (5, 44)
Cx43	Connexin 43	KO	Abnormal QRS (45, 46)
Cx45	Connexin 45	KO	*Isolated AV conduction block* (26, 47)
Hadhb	HAC-CoA-dehyd.	ENU	AV block with sudden death (48)
Kcnq1	K channel Q1	KO	Prolonged QT; abnormal QRS (49)
LmnA	Lamin A	KI	Abnormal QRS (50)
Nkx2-5	NK2 TF related 5	KO	Prolonged PR in hetero, lack of AV node in KO (51, 52)
Scn5A	Na channel Vα	KO	Prolonged P; tachycardia (36, 53, 54)
Tbx5	T-box5	KO	AV block, abnormal QRS, ventricular tachycardia (55, 56)
Agtr1a	Ang II - Receptor	TG	Abnormal QRS (57)
Tead4	TEA domain 4	TG	Abnormal QRS (58)
Vegfb	VEGF B	KO	*Isolated AV block* (*first degree only*) (59)

Italics show animal models that show the identical phenotype to the one described in this paper. ENU, ENU Mutagenesis screen; HAC-CaA dehyd., hydroxyacyl–Coenzyme A dehydrogenase; KI, knockin; TG, transgenic.

connexins in ventricle is comparable to the mechanism of action of N-cadherin in cardiac conduction defects. The documented changes in conduction could explain both the AV block and Sick sinus syndrome. It is important to note that different connexins are expressed in the conduction system and the myocardium. Furthermore, our preliminary expression profiling analysis indicated that the regulation of connexin expression in response to the loss of CAR differs between atrium and ventricle. Thus, altered communication of connexins can differentially affect the conduction system (AV block and Sick sinus syndrome) and the ventricle where the defect is compensated with no indication for electrical abnormalities but increased coupling.

Toward understanding the molecular basis of the isolated AV block, we would envision a mechanism where the loss of CAR results in an altered protein composition of the tight junction, as documented by our expression and immunofluorescence analysis (Figs. 6 and 7). Although the tight junction as a whole is not affected with normal ultrastructure and proper sublocalization of N-cadherin, we see connexins specifically respond to the loss of CAR with redistribution away from the intercalated disc and reduced protein levels (potentially a combination of reduced expression and degradation of mislocalized protein). The AV node shows less compartmentalization and a more homogenous distribution of CAR along the plasma membrane (Fig. 3). This would explain the isolated effect on the AV node where no predetermined structure, such as the intercalated disc, would facilitate proper electrical conduction.

Multiple diseases have been associated with the tight junction, ranging from deafness and cancer to allergies and infections (for review see reference 29). In this paper, we describe a novel role for the tight junction in arrhythmia. Not only does this have implications for CAR as a potential diagnostic marker for familial cases of AV block but it might also help explain how virus proteins or autoantibodies that interact with tight junction proteins, such as CAR, can cause arrhythmia (30). Shedding of virus proteins from infected cells is an important mechanism to disrupt CAR–CAR interaction at the tight junction and facilitate virus passing epithelial barriers (31). In the heart, this virus-induced disruption of CAR dimers would be expected to produce the same effect as the loss of CAR and, thus, ultimately lead to uncoupling and electrical conduction defects, which can accompany viral myocarditis (32). Autoantibodies in rheumatic women have been shown to cause AV block by disregulating Ca^{2+} homeostasis in cardiomyocytes (33). A similar mechanism could result from autoantibodies that interfere with tight junction proteins.

In conclusion, we have identified a novel mechanism for cardiac arrhythmia that involves the tight junction and results from loss of CAR, which is required to maintain functional gap junctions at the intercalated disc. Although the loss of CAR is well compensated in the myocardium, the altered electrical properties of the AV node result in a progressive AV block. At this time, there is no genetic defect of CAR associated with human disease, but our findings would suggest tight junction proteins as potential disease genes in genetic forms of isolated AV block. Furthermore, the role of CAR in arrhythmogenesis has implications for CVB3 infection and patients with heart disease resulting from antibodies against proteins of the tight junction, which may lead to better screening methods to identify persons at risk of potentially fatal arrhythmia and possibly to novel therapies.

MATERIALS AND METHODS

Generation of constitutive and inducible heart-specific CAR KO mice. To generate CAR-deficient animals, the Cre–lox recombination system was used, flanking CAR exon 1, which contains the ATG, with lox sites (Fig. 1 A). After homologous recombination, blastocyst injection of targeted embryonic stem cells was used to obtain KO animals. The neomycin/flp

resistance cassette was removed by germline expression of the FLP recombinase (34). Subsequently, we generated a constitutive and an inducible heart-specific CAR KO with the α-MHC promoter driving the expression of the nuclear-localized cre recombinase or the MerCreMer fusion protein, respectively (MerCreMer transgenic mice were provided by J. Molkentin, Cincinnati Children's Hospital Medical Center, Cincinnati, OH). Induction of MerCreMer with tamoxifen (30 mg per kilogram of body weight per day) has been described previously (18). We injected mice at 2 mo of age with 10 μg/μl of a solution of tamoxifen in peanut oil with five injections per week for 2 consecutive wk (10 injections; 300 mg/kg total). All experiments involving animals were performed according to institutional and National Institutes of Health guidelines (Using Animals in Intramural Research) and had been approved by the local authorities (LaGeSo Berlin).

Real-time PCR. Total RNA of the mouse left ventricle was isolated with TRIZOL (Invitrogen) and was purified using the RNeasy Mini kit (QIAGEN), followed by cDNA synthesis using Thermoscript First-Strand Synthesis System according to the manufacturer's instructions (Invitrogen). Primers probe sets (FAM and TAMRA labels) were ordered as Taqman Gene Expression Assays (Applied Biosystems), except for CAR and GAPDH (BioTeZ GmbH). The probe sets for CAR and GAPDH are the following: CAR, AGCTGCACGGTTCAAAACAGA (forward), TTCCGGCTCGGTTGGA (reverse), and 6-FAM-CTCTGACCAGTGTATGCTGCGACTAGACGT-TAMRA (probe); and GAPDH, GGCAAATTCAACGGCACAGT (forward), AGATGGTGATGGGCTTCCC (reverse), and 6-FAM-AGGCCGAGAATGGGAAGCTTGTCATC-TAMRA (probe). Amplification reaction and analysis has been previously described (35).

SDS-Page and Western blot. Protein preparation (three hearts per group), SDS PAGE, and Western blot have been previously described (35). Primary antibodies used against CAR (rabbit polyclonal; Santa Cruz Biotechnology, Inc.), α-actin (rabbit polyclonal; Sigma-Aldrich), Cx40 (rabbit polyclonal; Santa Cruz Biotechnology, Inc.), Cx45 (mouse monoclonal; Invitrogen), and GAPDH (mouse monoclonal; Affinity BioReagents) were used according to the manufacturer's instructions and detected with HRP-conjugated secondary antibodies and chemiluminescence staining using ECL (Supersignal West Pico Chemiluminescent Substrate; Thermo Fisher Scientific). Quantification was performed with the Image Analyzer software (v 4.19; AIDA).

Surface ECG and in vivo electrophysiology (EP) studies. Each mouse was lightly anesthetized with isoflorane (1.6 vol% isoflorane/air), and ECG standard intervals were measured in six-limb leads as described previously (36) ($n = 16$). The severity of the AV conduction defect was graded according to standard clinical diagnostic criteria. As AV block first degree is not defined for mouse, we based our classification on the distribution of PR intervals in our control group (mean + 2× SD). Thus, PR intervals >48 ms were considered as prolonged. Additional intermittent block of a single AV conduction was classified as AV block second degree. Third degree (complete) heart block was diagnosed when no atrial impulse propagated to the ventricles.

In vivo EP studies ($n = 21$) with programmed electrical stimulations were performed to assess standard parameters of atrial and ventricular conduction, refractoriness, and the inducibility of arrhythmia (37, 38). We used a digital EP laboratory (EP Tracer; CardioTek). During inhalation anesthesia with isoflorane at constant body temperature, an octapolar 2-French electrode catheter (CIBer mouse cath; NuMed, Inc.) was placed via the right jugular vein into the right atrium and ventricle, guided by the morphology of intracardiac electrical signals. Impulses were delivered at twice diastolic threshold with a pulse duration of 1 ms. To test for inducibility of arrhythmias, the programmed ventricular stimulation protocols included trains of 10 basal stimuli (S1, cl 90/100/120 ms) followed by up to three extrastimuli (S2–S4), delivered with a coupling interval decreasing in steps of 5 ms until ventricular refractoriness was reached. Additional short episodes of burst pacing with cycle lengths down to 60 ms were applied. Only reproducible arrhythmias up from three beats were considered.

For continuous ECG monitoring, ECG radiotransmitters (TA10ETA-F20; DSI, Inc.) were implanted under isoflurane anesthesia. The body of the implant was placed subcutaneously at the back of the animals. The two leads were fixed subcutaneously in a standard lead II position (right upper and left lower thorax). After surgery, the mice (WT, $n = 3$; CAR KO, $n = 3$) were housed individually in cages placed over radio receivers (CTR85-SA; DSI, Inc.). Initial ECG parameters were obtained after 1 wk of recovery from surgery before the start of tamoxifen injections.

Histology and electron microscopy. For histology, hearts were aseptically removed and fixed for 12 h in phosphate-buffered (pH 7.2) 4% paraformaldehyde and embedded in paraffin. 5-μm sections were deparaffinized and stained with Masson's Trichrome (Sigma-Aldrich) to detect the fibrous body. AChE (acetylcholinesterase) staining to identify the AV node was performed on cryosections from hearts perfused with 4% paraformaldehyde, equilibrated with 30% sucrose, and embedded in OCT (Sakura). The staining procedure was adapted from El-Badawi and Schenk (39). Ultrastructural analysis was according to our published protocol (35).

Three-dimensional reconstruction of the AV node. Serial sections (5 μm) covering the complete AV node were collected and any loss of sections was noted. The three-dimensional reconstruction of the dataset was created using the Meta Imaging Series Software (MDS Analytical Technologies). Each image section was aligned and stacked one on top of another to create a three-dimensional volume calculated using the three-dimensional reconstruction tool of MetaMorph 7.1.7.

Immunofluorescence and immunohistochemistry analysis. Cardiomyocytes were isolated from heart ventricles as described previously (40), seeded to laminin-coated glass coverslips for 4 h, and fixed with cold methanol. For immunofluorescence staining, we followed the published protocol (35). The primary antibodies used were the following: rat anti-HCN4 (Abcam) and anti-CAR (rabbit polyclonal, raised against the Fc fusion protein containing the CA extracellular domain), anti-CAR (rabbit polyclonal; Santa Cruz Biotechnology, Inc.), anti–N-cadherin (mouse monoclonal; Invitrogen), anti-Cx43 (mouse monoclonal; Invitrogen), and anti–α-actinin (mouse monoclonal; Sigma-Aldrich). Fluorescent-conjugated secondary antibodies were the following: goat anti–rat Alexa Fluor 555 (Invitrogen), goat anti–rabbit Alexa Fluor 647 (Invitrogen), goat anti–rat Alexa Fluor 488 (Invitrogen), goat anti–mouse Alexa Fluor 647 (Invitrogen), and goat anti–rabbit Alexa Fluor 568 (Invitrogen).

For ChAT immunohistochemistry, paraffin sections were deparaffinized, demasked, and blocked before incubation with goat anti-ChAT antibody over night (Millipore). After incubation with donkey anti–goat biotin-conjugated secondary antibody (Jackson ImmunoResearch Laboratories) followed by the ABC Elite reagent (Vector Laboratories), sections were developed with DAB (Dako) and counterstained with hematoxylin (Sigma-Aldrich).

Preparation of cardiac muscle slices and dye-coupling studies. Hearts at the indicated times were quickly removed after cervical dislocation under deep ether anesthesia and transferred to ice-cold oxygenated standard salt solution containing the following: 125 mM NaCl, 4 mM KCl, 10 mM glucose, 1.25 mM NaH_2PO_4, 25 mM $NaHCO_3$, 2 mM $CaCl_2$, and 1 mM $MgCl_2$. Ventricles were longitudinally cut and embedded in 2.5% low melting temperature agarose (Biozym Scientific GmbH) at 30°C. The blocks were glued to the stage of a vibrating blade microtome (Leica) and 250 μm-slices were prepared.

To examine gap junctional coupling, slices were transferred into a submerged recording chamber. Glass capillaries prepared by a puller (P-97; Sutter Instrument Co.) were filled with 2% (wt/vol) 6-carboxyfluorescein (Sigma-Aldrich). The pipette resistance was 30–40 MOhm. Pipette solution contained 120 mM KCl, 4 mM NaCl, 5 mM glucose, 5 mM EGTA, 10 mM Hepes, 0.5 mM $CaCl_2$, and 4 mM $MgCl_2$, pH 7.3.

The cardiomyocytes were selected according to the following criteria: first, the dye diffused into the initial cell within the first minute; second, the

rectangular shape could be recognized; third, the cell should be localized within a fiber; and fourth, the fiber displayed apparently regular contraction. Individual cardiomyocytes were injected with the dye by iontophoretic injection for 4 min taking negative voltage pulses of 0.8 V (duration 500 ms, 1 Hz) using EPC-9 (HEKA Elektronik). Intracellular communication was monitored under fluorescence microscopy and optical images recorded by a charge-coupled device camera (AxioCam HRC; Carl Zeiss, Inc.). For fluorescence images, filter set 46 was used (Zeiss; excitation, 500/20 nm; filtration, 515 nm; emission, 535/30 nm). The area of dye spread was quantified by BioVision software (BioVision, Inc.). The investigator was blinded to the genotype.

Statistics. For statistical analysis, Prism 5.0 software (GraphPad Software, Inc.) was used. Results are expressed as means ± SEM. Statistical significance between groups was determined using the Mann Whitney U test for hemodynamic and EP data. Expression values were compared using an unpaired two-tailed *t* test to assess differences between two groups. The significance level was chosen as $P = 0.05$.

Online supplemental material. In vivo recordings of the cardiac electrical activity by EPU and telemetry document the progression of the arrhythmia, the response to isoproterenol, and changes in heart rate after induction of the phenotype (Figs. S1–4). Ultrastructure of the KO cardiac sarcomere and intercalated disc is not significantly altered upon loss of CAR (Fig. S5). Online supplemental material is available at http://www.jem.org/cgi/content/full/jem.20080897/DC1.

We thank Dr. Jeffrey Molkentin for the MerCreMer transgenic mice. We are grateful to Beate Goldbrich, Mandy Terne, and Carolin Schmidt for expert technical assistance and Ralph Plehm and Reika Langangki for their support with the telemetry.

This study was supported by the Deutsche Forschungsgemeinschaft (SFB TR19).

The authors have no conflicting financial interests.

Submitted: 23 April 2008
Accepted: 13 August 2008

REFERENCES

1. Tomaselli, G.F., D.J. Beuckelmann, H.G. Calkins, R.D. Berger, P.D. Kessler, J.H. Lawrence, D. Kass, A.M. Feldman, and E. Marban. 1994. Sudden cardiac death in heart failure. The role of abnormal repolarization. *Circulation*. 90:2534–2539.
2. Saffitz, J.E., J.G. Laing, and K.A. Yamada. 2000. Connexin expression and turnover: implications for cardiac excitability. *Circ. Res*. 86:723–728.
3. Peters, N.S. 2006. Gap junctions: clarifying the complexities of connexins and conduction. *Circ. Res*. 99:1156–1158.
4. Kreuzberg, M.M., K. Willecke, and F.F. Bukauskas. 2006. Connexin-mediated cardiac impulse propagation: connexin 30.2 slows atrioventricular conduction in mouse heart. *Trends Cardiovasc. Med*. 16:266–272.
5. Simon, A.M., D.A. Goodenough, and D.L. Paul. 1998. Mice lacking connexin40 have cardiac conduction abnormalities characteristic of atrioventricular block and bundle branch block. *Curr. Biol*. 8:295–298.
6. Li, J., V.V. Patel, I. Kostetskii, Y. Xiong, A.F. Chu, J.T. Jacobson, C. Yu, G.E. Morley, J.D. Molkentin, and G.L. Radice. 2005. Cardiac-specific loss of N-cadherin leads to alteration in connexins with conduction slowing and arrhythmogenesis. *Circ. Res*. 97:474–481.
7. Oxford, E.M., H. Musa, K. Maass, W. Coombs, S.M. Taffet, and M. Delmar. 2007. Connexin43 remodeling caused by inhibition of plakophilin-2 expression in cardiac cells. *Circ. Res*. 101:703–711.
8. Cohen, C.J., J.T. Shieh, R.J. Pickles, T. Okegawa, J.T. Hsieh, and J.M. Bergelson. 2001. The coxsackievirus and adenovirus receptor is a transmembrane component of the tight junction. *Proc. Natl. Acad. Sci. USA*. 98:15191–15196.
9. Bergelson, J.M., J.A. Cunningham, G. Droguett, E.A. Kurt-Jones, A. Krithivas, J.S. Hong, M.S. Horwitz, R.L. Crowell, and R.W. Finberg. 1997. Isolation of a common receptor for Coxsackie B viruses and adenoviruses 2 and 5. *Science*. 275:1320–1323.
10. Tomko, R.P., R. Xu, and L. Philipson. 1997. HCAR and MCAR: the human and mouse cellular receptors for subgroup C adenoviruses and group B coxsackieviruses. *Proc. Natl. Acad. Sci. USA*. 94:3352–3356.
11. Sollerbrant, K., E. Raschperger, M. Mirza, U. Engstrom, L. Philipson, P.O. Ljungdahl, and R.F. Pettersson. 2003. The Coxsackievirus and adenovirus receptor (CAR) forms a complex with the PDZ domain-containing protein ligand-of-numb protein-X (LNX). *J. Biol. Chem*. 278:7439–7444.
12. Coyne, C.B., T. Voelker, S.L. Pichla, and J.M. Bergelson. 2004. The coxsackievirus and adenovirus receptor interacts with the multi-PDZ domain protein-1 (MUPP-1) within the tight junction. *J. Biol. Chem*. 279:48079–48084.
13. Chung, S.K., J.Y. Kim, I.B. Kim, S.I. Park, K.H. Paek, and J.H. Nam. 2005. Internalization and trafficking mechanisms of coxsackievirus B3 in HeLa cells. *Virology*. 333:31–40.
14. Asher, D.R., A.M. Cerny, S.R. Weiler, J.W. Horner, M.L. Keeler, M.A. Neptune, S.N. Jones, R.T. Bronson, R.A. Depinho, and R.W. Finberg. 2005. Coxsackievirus and adenovirus receptor is essential for cardiomyocyte development. *Genesis*. 42:77–85.
15. Dorner, A.A., F. Wegmann, S. Butz, K. Wolburg-Buchholz, H. Wolburg, A. Mack, I. Nasdala, B. August, J. Westermann, F.G. Rathjen, and D. Vestweber. 2005. Coxsackievirus-adenovirus receptor (CAR) is essential for early embryonic cardiac development. *J. Cell Sci*. 118:3509–3521.
16. Chen, J.W., B. Zhou, Q.C. Yu, S.J. Shin, K. Jiao, M.D. Schneider, H.S. Baldwin, and J.M. Bergelson. 2006. Cardiomyocyte-specific deletion of the coxsackievirus and adenovirus receptor results in hyperplasia of the embryonic left ventricle and abnormalities of sinuatrial valves. *Circ. Res*. 98:923–930.
17. Agah, R., P.A. Frenkel, B.A. French, L.H. Michael, P.A. Overbeek, and M.D. Schneider. 1997. Gene recombination in postmitotic cells. Targeted expression of Cre recombinase provokes cardiac-restricted, site-specific rearrangement in adult ventricular muscle in vivo. *J. Clin. Invest*. 100:169–179.
18. Peng, J., K. Raddatz, J.D. Molkentin, Y. Wu, S. Labeit, H. Granzier, and M. Gotthardt. 2007. Cardiac hypertrophy and reduced contractility in hearts deficient in the titin kinase region. *Circulation*. 115:743–751.
19. Nikolski, V.P., S.A. Jones, M.K. Lancaster, M.R. Boyett, and I.R. Efimov. 2003. Cx43 and dual-pathway electrophysiology of the atrioventricular node and atrioventricular nodal reentry. *Circ. Res*. 92:469–475.
20. Ciray, H.N., B.E. Persson, G.M. Roomans, and U. Ulmsten. 1995. Dye-coupling between term pregnant human myometrial cells before labor: carboxyfluorescein versus lucifer yellow. *Cell Biol. Int*. 19:609–617.
21. Toyofuku, T., M. Yabuki, K. Otsu, T. Kuzuya, M. Hori, and M. Tada. 1998. Direct association of the gap junction protein connexin-43 with ZO-1 in cardiac myocytes. *J. Biol. Chem*. 273:12725–12731.
22. Thoelen, I., C. Magnusson, S. Tagerud, C. Polacek, M. Lindberg, and M. Van Ranst. 2001. Identification of alternative splice products encoded by the human coxsackie-adenovirus receptor gene. *Biochem. Biophys. Res. Commun*. 287:216–222.
23. Dorner, A., D. Xiong, K. Couch, T. Yajima, and K.U. Knowlton. 2004. Alternatively spliced soluble coxsackie-adenovirus receptors inhibit coxsackievirus infection. *J. Biol. Chem*. 279:18497–18503.
24. Nguyen, H.H., J.T. Wolfe III, D.R. Holmes Jr., and W.D. Edwards. 1988. Pathology of the cardiac conduction system in myotonic dystrophy: a study of 12 cases. *J. Am. Coll. Cardiol*. 11:662–671.
25. Nagasawa, K., H. Chiba, H. Fujita, T. Kojima, T. Saito, T. Endo, and N. Sawada. 2006. Possible involvement of gap junctions in the barrier function of tight junctions of brain and lung endothelial cells. *J. Cell. Physiol*. 208:123–132.
26. Nishii, K., M. Kumai, K. Egashira, T. Miwa, K. Hashizume, Y. Miyano, and Y. Shibata. 2003. Mice lacking connexin45 conditionally in cardiac myocytes display embryonic lethality similar to that of germline knockout mice without endocardial cushion defect. *Cell Commun. Adhes*. 10:365–369.
27. Bagwe, S., O. Berenfeld, D. Vaidya, G.E. Morley, and J. Jalife. 2005. Altered right atrial excitation and propagation in connexin40 knockout mice. *Circulation*. 112:2245–2253.
28. Danik, S.B., G. Rosner, J. Lader, D.E. Gutstein, G.I. Fishman, and G.E. Morley. 2007. Electrical remodeling contributes to complex tachyarrhythmias in connexin43-deficient mouse hearts. *FASEB J*. 22:1204–1212.

29. Cereijido, M., R.G. Contreras, D. Flores-Benitez, C. Flores-Maldonado, I. Larre, A. Ruiz, and L. Shoshani. 2007. New diseases derived or associated with the tight junction. *Arch. Med. Res.* 38:465–478.
30. Sato, Y., A. Osaku, S. Koyama, S. Mizukawa, S. Onikura, H. Yagi, T. Suzuki, T. Sawada, T. Uchiyama, and K. Kanmatsuse. 1989. Complete atrioventricular block associated with regional myocardial scarring in a patient with Coxsackie B2 myocarditis. *Jpn. Heart J.* 30:935–941.
31. Walters, R.W., P. Freimuth, T.O. Moninger, I. Ganske, J. Zabner, and M.J. Welsh. 2002. Adenovirus fiber disrupts CAR-mediated intercellular adhesion allowing virus escape. *Cell.* 110:789–799.
32. Kishimoto, C., A. Matsumori, M. Ohmae, N. Tomioka, and C. Kawai. 1984. Electrocardiographic findings in experimental myocarditis in DBA/2 mice: complete atrioventricular block in the acute stage, low voltage of the QRS complex in the subacute stage and arrhythmias in the chronic stage. *J. Am. Coll. Cardiol.* 3:1461–1468.
33. Salomonsson, S., S.E. Sonesson, L. Ottosson, S. Muhallab, T. Olsson, M. Sunnerhagen, V.K. Kuchroo, P. Thoren, E. Herlenius, and M. Wahren-Herlenius. 2005. Ro/SSA autoantibodies directly bind cardiomyocytes, disturb calcium homeostasis, and mediate congenital heart block. *J. Exp. Med.* 201:11–17.
34. Gotthardt, M., R.E. Hammer, N. Hubner, J. Monti, C.C. Witt, M. McNabb, J.A. Richardson, H. Granzier, S. Labeit, and J. Herz. 2003. Conditional expression of mutant M-line titins results in cardiomyopathy with altered sarcomere structure. *J. Biol. Chem.* 278:6059–6065.
35. Weinert, S., N. Bergmann, X. Luo, B. Erdmann, and M. Gotthardt. 2006. M line–deficient titin causes cardiac lethality through impaired maturation of the sarcomere. *J. Cell Biol.* 173:559–570.
36. Royer, A., T.A. van Veen, B.S. Le, C. Marionneau, V. Griol-Charhbili, A.L. Leoni, M. Steenman, H.V. van Rijen, S. Demolombe, C.A. Goddard, et al. 2005. Mouse model of SCN5A-linked hereditary Lenegre's disease: age-related conduction slowing and myocardial fibrosis. *Circulation.* 111:1738–1746.
37. Berul, C.I., M.E. Christe, M.J. Aronovitz, C.E. Seidman, J.G. Seidman, and M.E. Mendelsohn. 1997. Electrophysiological abnormalities and arrhythmias in alpha MHC mutant familial hypertrophic cardiomyopathy mice. *J. Clin. Invest.* 99:570–576.
38. VanderBrink, B.A., M.S. Link, M.J. Aronovitz, S. Saba, S.B. Sloan, M.K. Homoud, N.A. Estes III, and P.J. Wang. 1999. Assessment of atrioventricular nodal physiology in the mouse. *J. Interv. Card. Electrophysiol.* 3:207–212.
39. El-Badawi, A., and E.A. Schenk. 1967. Histochemical methods for separate, consecutive and simultaneous demonstration of acetylcholinesterase and norepinephrine in cryostat sections. *J. Histochem. Cytochem.* 15:580–588.
40. Radke, M.H., J. Peng, Y. Wu, M. McNabb, O.L. Nelson, H. Granzier, and M. Gotthardt. 2007. Targeted deletion of titin N2B region leads to diastolic dysfunction and cardiac atrophy. *Proc. Natl. Acad. Sci. USA.* 104:3444–3449.
41. Platzer, J., J. Engel, A. Schrott-Fischer, K. Stephan, S. Bova, H. Chen, H. Zheng, and J. Striessnig. 2000. Congenital deafness and sinoatrial node dysfunction in mice lacking class D L-type Ca2+ channels. *Cell.* 102:89–97.
42. Chen, B., R.T. Bronson, L.D. Klaman, T.G. Hampton, J.F. Wang, P.J. Green, T. Magnuson, P.S. Douglas, J.P. Morgan, and B.G. Neel. 2000. Mice mutant for Egfr and Shp2 have defective cardiac semilunar valvulogenesis. *Nat. Genet.* 24:296–299.
43. Stephen, L.J., A.L. Fawkes, A. Verhoeve, G. Lemke, and A. Brown. 2007. A critical role for the EphA3 receptor tyrosine kinase in heart development. *Dev. Biol.* 302:66–79.
44. Kirchhoff, S., E. Nelles, A. Hagendorff, O. Kruger, O. Traub, and K. Willecke. 1998. Reduced cardiac conduction velocity and predisposition to arrhythmias in connexin40-deficient mice. *Curr. Biol.* 8:299–302.
45. Reaume, A.G., P. A.de Sousa, S. Kulkarni, B.L. Langille, D. Zhu, T.C. Davies, S.C. Juneja, G.M. Kidder, and J. Rossant. 1995. Cardiac malformation in neonatal mice lacking connexin43. *Science.* 267:1831–1834.
46. Flenniken, A.M., L.R. Osborne, N. Anderson, N. Ciliberti, C. Fleming, J.E. Gittens, X.Q. Gong, L.B. Kelsey, C. Lounsbury, L. Moreno, et al. 2005. A Gja1 missense mutation in a mouse model of oculodentodigital dysplasia. *Development.* 132:4375–4386.
47. Kumai, M., K. Nishii, K. Nakamura, N. Takeda, M. Suzuki, and Y. Shibata. 2000. Loss of connexin45 causes a cushion defect in early cardiogenesis. *Development.* 127:3501–3512.
48. Kao, H.J., C.F. Cheng, Y.H. Chen, S.I. Hung, C.C. Huang, D. Millington, T. Kikuchi, J.Y. Wu, and Y.T. Chen. 2006. ENU mutagenesis identifies mice with cardiac fibrosis and hepatic steatosis caused by a mutation in the mitochondrial trifunctional protein beta-subunit. *Hum. Mol. Genet.* 15:3569–3577.
49. Casimiro, M.C., B.C. Knollmann, S.N. Ebert, J.C. Vary Jr., A.E. Greene, M.R. Franz, A. Grinberg, S.P. Huang, and K. Pfeifer. 2001. Targeted disruption of the Kcnq1 gene produces a mouse model of Jervell and Lange-Nielsen Syndrome. *Proc. Natl. Acad. Sci. USA.* 98:2526–2531.
50. Arimura, T., A. Helbling-Leclerc, C. Massart, S. Varnous, F. Niel, E. Lacene, Y. Fromes, M. Toussaint, A.M. Mura, D.I. Keller, et al. 2005. Mouse model carrying H222P-Lmna mutation develops muscular dystrophy and dilated cardiomyopathy similar to human striated muscle laminopathies. *Hum. Mol. Genet.* 14:155–169.
51. Biben, C., R. Weber, S. Kesteven, E. Stanley, L. McDonald, D.A. Elliott, L. Barnett, F. Koentgen, L. Robb, M. Feneley, and R.P. Harvey. 2000. Cardiac septal and valvular dysmorphogenesis in mice heterozygous for mutations in the homeobox gene Nkx2-5. *Circ. Res.* 87:888–895.
52. Jay, P.Y., B.S. Harris, C.T. Maguire, A. Buerger, H. Wakimoto, M. Tanaka, S. Kupershmidt, D.M. Roden, T.M. Schultheiss, T.X. O'Brien, et al. 2004. Nkx2-5 mutation causes anatomic hypoplasia of the cardiac conduction system. *J. Clin. Invest.* 113:1130–1137.
53. Papadatos, G.A., P.M. Wallerstein, C.E. Head, R. Ratcliff, P.A. Brady, K. Benndorf, R.C. Saumarez, A.E. Trezise, C.L. Huang, J.I. Vandenberg, et al. 2002. Slowed conduction and ventricular tachycardia after targeted disruption of the cardiac sodium channel gene Scn5a. *Proc. Natl. Acad. Sci. USA.* 99:6210–6215.
54. Remme, C.A., A.O. Verkerk, D. Nuyens, A.C. van Ginneken, S. van Brunschott, C.N. Belterman, R. Wilders, M.A. van Roon, H.L. Tan, A.A. Wilde, P. Carmeliet, J.M. de Bakker, M.W. Veldkamp, and C.R. Bezzina. 2006. Overlap syndrome of cardiac sodium channel disease in mice carrying the equivalent mutation of human SCN5A-1795insD. *Circulation.* 114:2584–2594.
55. Moskowitz, I.P., A. Pizard, V.V. Patel, B.G. Bruneau, J.B. Kim, S. Kupershmidt, D. Roden, C.I. Berul, C.E. Seidman, and J.G. Seidman. 2004. The T-Box transcription factor Tbx5 is required for the patterning and maturation of the murine cardiac conduction system. *Development.* 131:4107–4116.
56. Mori, A.D., Y. Zhu, I. Vahora, B. Nieman, K. Koshiba-Takeuchi, L. Davidson, A. Pizard, J.G. Seidman, C.E. Seidman, X.J. Chen, et al. 2006. Tbx5-dependent rheostatic control of cardiac gene expression and morphogenesis. *Dev. Biol.* 297:566–586.
57. Hein, L., M.E. Stevens, G.S. Barsh, R.E. Pratt, B.K. Kobilka, and V.J. Dzau. 1997. Overexpression of angiotensin AT1 receptor transgene in the mouse myocardium produces a lethal phenotype associated with myocyte hyperplasia and heart block. *Proc. Natl. Acad. Sci. USA.* 94:6391–6396.
58. Chen, H.H., C.J. Baty, T. Maeda, S. Brooks, L.C. Baker, T. Ueyama, E. Gursoy, S. Saba, G. Salama, B. London, and A.F. Stewart. 2004. Transcription enhancer factor-1-related factor-transgenic mice develop cardiac conduction defects associated with altered connexin phosphorylation. *Circulation.* 110:2980–2987.
59. Aase, K., G. von Euler, X. Li, A. Ponten, P. Thoren, R. Cao, Y. Cao, B. Olofsson, S. Gebre-Medhin, M. Pekny, K. Alitalo, C. Betsholtz, and U. Eriksson. 2001. Vascular endothelial growth factor-B-deficient mice display an atrial conduction defect. *Circulation.* 104:358–364.